Vol. 23, No. 3(2024) Sim24267
Revista Mexicana de Ingeniería Química

Numerical and experimental study of a fluidic oscillator

Estudio numérico y experimental de un oscilador fluídico

R. Gonzalez-Mora[1], S. A. Arreola-Villa[2], B. Figueroa-Espinoza[3], S.R. Galvan-Gonzalez[1], A. Aguilar-Corona[1]*
[1] *Facultad de Ingeniería Mecánica, Universidad Michoacana de San Nicolás de Hidalgo, Francisco J. Múgica S/N, Ciudad Universitaria, 58030, Morelia, Michoacán, México.*
[2] *Facultad de Ingeniería Mecánica y Eléctrica, Universidad Autónoma de Coahuila, Barranquillas S/N, Col. Guadalupe, Monclova 25280, México.*
[3] *LIPC-Instituto de Ingeniería UNAM, Puerto de Abrigo S/N 97355, Yucatán, México.*
Received: February 13, 2024; Accepted: April 28, 2024

Abstract
Fluidics is a discipline that uses physics of fluids to produce output signals similar to those used in electronics, such as logical operations or oscillations for a wide variety of applications. Most devices have no moving parts and are relatively easy to produce. This investigation uses 3D Direct Numerical Simulations (DNS) and an experimental prototype to characterize a fluidic oscillator. The geometrical design (man-shaped) causes a self-sustained switching between two outlets. Two important vortices were identified, related to the output selection: one small vortex near one of the control ports (Coanda effect), responsible for the switching, and a larger one on the mixing zone (belly), facilitating the flow towards the opposite side. The oscillation frequency for the experimental prototype was determined by the application of a Fast Fourier transform of the output signal, captured with a microphone. The onset of the oscillations, as well as the frequencies in terms of the Strouhal (*Sr*) and Reynolds (*Re*) numbers were obtained. The *Sr* is a monotonically increasing function Re, up to a transition Reynolds number (maximum) where *Sr* starts decreasing with Re (at quasi-constant frequency). The numerical simulation results were in agreement with the experiments, and allowed for the visualization of the mechanisms responsible for the switching. These results suggest that numerical techniques can be used for design purposes in fluidics.
Keywords: Fluidic Oscillator, Coanda Effect, DNS, Fluidics.

Resumen
La fluídica es una disciplina que utiliza la física de los fluidos para producir señales de salida similares a las utilizadas en electrónica, como operaciones lógicas u oscilaciones para una amplia variedad de aplicaciones. La mayoría de los dispositivos no tienen partes móviles y son relativamente fáciles de producir. Esta investigación utiliza Simulaciones Numéricas Directas (DNS) en 3D y un prototipo experimental para caracterizar un oscilador fluídico. El diseño geométrico del oscilador tiene una geometría en forma de hombre. Este dispositivo provoca una oscilación autosostenible entre las dos salidas. Se identificaron dos vórtices importantes que provocan la oscilación: un pequeño vórtice cerca de uno de los puertos de control (efecto Coanda) y uno más grande en la zona de mezcla (vientre), que facilita el flujo hacia el lado opuesto. La frecuencia de oscilación del prototipo experimental se determinó mediante la aplicación de una transformada rápida de Fourier de la señal de salida, capturada con un micrófono. Se caracteriza el funcionamiento del dispositivo en términos de los números de Strouhal (Sr) y Reynolds (Re). El Sr es una función Re que aumenta monótonamente, hasta un número de Reynolds de transición (máximo) donde Sr comienza a disminuir con el Re (a una frecuencia casi constante). Los resultados de la simulación numérica coincidieron con los experimentos y permitieron la visualización de los mecanismos responsables de la oscilación. Los resultados obtenidos sugieren que las técnicas numéricas se pueden utilizar con fines de diseño en fluídica.
Palabras clave: Oscilador Fluídico, Efecto Coanda, DNS, Fluídico.

* *Corresponding author. E-mail*: alicia.aguilar@umich.mx;
https://doi.org/10.24275/rmiq/Sim24267
ISSN:1665-2738, *issn-e*: 2395-8472

1 Introduction

Active flow controls, fluid oscillators or also known as sweep jets, have the characteristic of converting a continuous flow into an oscillating and/or pulsating flow. Various classifications have been made, among which we highlight that of Gregory and Tomac (2013) who classify the oscillators according to the mechanisms that drive the oscillations: Jet-Interaction oscillators (Tomac and Gregory, 2014) and Wall attached fluidic oscillators (Schmidt et al., 2017; Tajik et al., 2021). In the first category, the mechanism consists of bringing two fluid jets into contact, causing instability within a mixing chamber, which causes the formation of vortices in different positions of the mixing chamber and finally produces an oscillating flow at the outlet of the device. Devices in the second category work based on the Coanda effect (Lubbert, 2011) where the geometry is an important factor. In general, for this case, the devices consist of a mixing chamber and a feedback channel, which is connected to the mixing chamber at two ends. As the fluid enters the mixing chamber, the main fluid jet adheres to one wall of the chamber and another part of the fluids transported by the feedback channel. The fluid that is transported in this channel produces pressure changes, detachment of the boundary layer and the formation of vortices in the mixing chamber that give rise to a continuous change in direction of the main jet. If there are no diverters at the outlet, the outlet flow will have a sweeping movement and if diverters exist, a pulsating flow will be obtained. The frequency and amplitude of this flow at the outlet is mainly attributed to the geometry, size and flow rate supplied (Bobusch et al., 2013). One of the main disadvantages of both systems is related to the mass flow of fluid that is necessary to give rise to the instability and pressure drop present in the system (Cerretelli & Kirtley, 2009). Various works have studied the effect of the oscillator geometry on the sweeping amplitude and the frequency of the fluid in order to improve its efficiency (Tajik et al., 2021; Loffler et al., 2021; Wen et al., 2020). However, more studies are necessary since fluidic oscillators are the most important passive alternatives to generate required pulsating or sweeping fluid flow patterns in the future (Ghanami and Mousa, 2019). Modern visualization and measurement techniques such as the Particle Image Velocimetry (Wen et al., 2020, Tomac, 2020; Mohammadshahi et al., 2019) and the hot-wire anemometer (Koklu, 2016) have been used to better understand the mechanism. The use of fluidics in the design of fluid flow control has several advantages with respect to mechanical and electronic devices (Lee, 1968). They require no moving parts, so there are no wearing or electrical problems, with minimum maintenance. Due to the mentioned characteristics, since the mid-20th century, the use of oscillators in the aerospace area has been studied (Campagnuolo & Lee, 1969; Griffin, 1966), with their current most popular application being windshield washer fluid nozzles (Gregory & Tomac, 2013), in flow separation control operations especially in the aeronautical sector (Cerretelli & Kirtley, 2009; Schmidt et al., 2017; Loffler et al., 2021; Whalen et al., 2018; Jentzsc et al., 2019; Woszidlo et al., 2010) and in heat and mass transfer (Kim, 2019; Mohammadshahi, 2019). Recent studies use this devices to produce microbubbles (Rehman et al., 2015), which can be used to enhance mass transfer in chemical and biological reactors (Quijano et al., 2020) as well as in the flotation of particles (López-Saucedo et al., 2016). The reason for this is that it is surprisingly difficult to produce small bubbles in a flow because of the effect of surface tension (Zimmerman et al., 2008; Zimmerman et al., 2009); to put it briefly, smaller bubbles have better retention times and transfer surface area ratio, i.e. heat/mass transfer is more efficient (Figueroa-Espinoza & Legendre, 2010; Devantine & Mietton-Peuchot, 2009). The design of such devices is usually based on trial-and-error experimentation. Although there exist some basic “rules of thumb” that help in the development of fluidic applications (Lee, 1968), each device is unique and requires extensive testing and re-design steps. These iterations can be less expensive if done numerically before prototyping is carried out. There exist many attempts to characterize fluidic devices in the literature, where the effect of compressibility can be taken into account (Gokoglu et al., 2010) and those where the Mach number does not require compressibility that may study the effects of the design on the output characteristics. Some simplifications apply, such as 2D simulations that match relatively well the dynamics observed experimentally, as well as the URANS approximation where turbulence cannot be ignored (Krüger et al., 2013; Bobusch et al., 2013; Jeong et al., 2017). Given the previous work's success on predicting the working conditions numerically, the present study proposes implementing Numerical Simulations of a fluidic oscillator to characterize the frequency-to-mass-flow-rate curves, as a pre-prototyping step for a microbubble production scheme. Likewise, the experimental study of the device is carried out in order to validate and complement the numerical study, in particular for high Re, where the simulation requires very high resolution or the use of turbulence models or empirical methods. It is important to explore the different flow regimes from both scientific and engineering purposes. The characteristics of the resulting oscillating outflow depend on two important numbers (Re and Sr). This study uses a combination of experimental and numerical tools to characterize these flow fields and corresponding regimes.

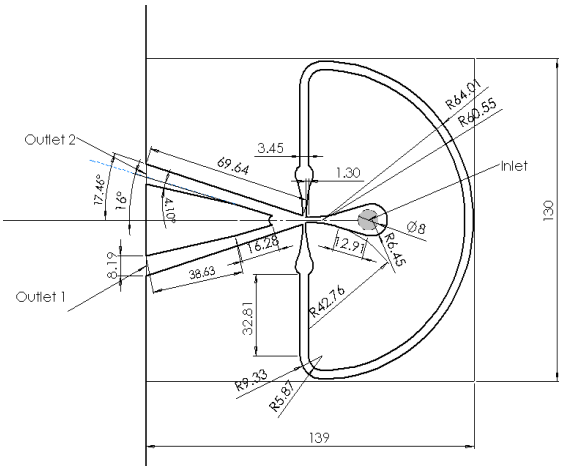

Figure 1. Scheme of the oscillator, scale in millimeters.

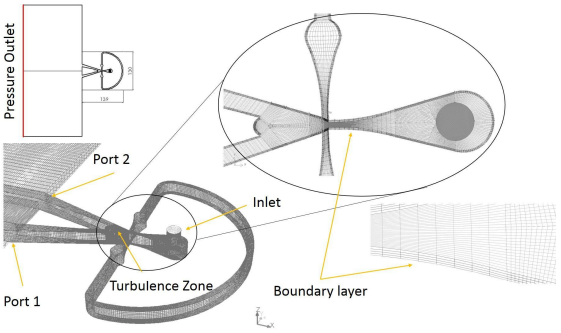

Figure 2. Meshing of the oscillator.

2 Methods

The fluidic oscillator performance relies on the Coanda effect (Lee, 1968). This effect can be used to redirect a jet back and forth through a couple of exit channels, creating a self-sustained oscillation triggered by a feedback loop. Figure 1 shows the geometry of the proposed device (units in mm) with a thickness of 8 mm (perpendicular to the plane). The device, which resembles a little man with open arms, consists of a head (air inlet), a body (mixing chamber), two arms (feedback channel), which are interconnected and serve the purpose of control ports, and two legs, which are the ports 1 and 2. The geometric design of the device is based on the work of Zimmerman et al (2008) and Kim (2011), with some design modifications. An oscillating cycle can be described as follows: firstly, the fluid enters the device through the inlet (head), perpendicular to the figure. The flow reaches the mixing chamber and bifurcates through the outlets (diverters). Since the symmetry of the flow is unstable, any perturbation on either side will cause the formation of (asymmetric) vortices in the mixing chamber, deviating most of the flow through one of the outlets, while almost blocking the other one (Coanda effect). This asymmetry of the pressure field causes a feedback flow through the control ports (the arms), which are connected, communicating the perturbation to the other side. This small perturbation takes some time to reach the other control port (arm). Once the perturbation reaches the other side (arm), it causes the jet to switch to the other port (leg), which in turn causes a feedback through the arms, restarting the cycle. The present study proposes the use of direct numerical simulations as a tool to shed some light on the performance of this system, whose complex behavior is difficult to assess using analytical tools. The operating conditions of the oscillator have been characterized using direct numerical simulation, and validated using a 3D printed prototype in the laboratory.

2.1 *Governing equations and numerical method*

The mass and momentum conservation equations for an incompressible liquid of density ρ and constant viscosity μ were considered:

$$\nabla \cdot \mathbf{v} = 0 \tag{1}$$

$$\rho\left(\frac{\partial \mathbf{v}}{\partial t} + \mathbf{v} \cdot \nabla \mathbf{v}\right) = -\nabla p + \mu \nabla^2 \mathbf{v} + \rho \mathbf{g} \tag{2}$$

where $\mathbf{v}$ is the velocity, p the pressure, $\mathbf{g}$ is the acceleration of gravity. The fluid properties are density $\rho = 1.225$ kgm^{-3}, and viscosity $\mu = 1.7894E - 05$ kg(mqs)$^{-1}$. The flow is unsteady and the selected method of discretization was Finite Volumes, given its intrinsic conservative properties and versatility in terms of representing the physical domain in a numerical grid (Moukalled et al., 2016). The unsteady simulation was carried out using a Semi Implicit Method for Pressure Linked Equations (SIMPLE, second order), which handless the pressure-velocity coupling using an iterative procedure that corrects for conservation of mass and momentum on each time step (Pantakar, 1980; Pantakar and Spalding, 1972). Direct Numerical Simulations were used in order to avoid the appearance of artificial recirculations, which have been observed when introducing turbulence models in similar problems. Moreover, for unsteady simulations it is common to observe serious inconsistencies when trying to predict recirculations and separation using turbulence models (Menter et al., 2003). The numerical tool used to solve the fluidic oscillator problem was ANSYS FLUENT®, which allows for both the numerical solver implementation as well as the complex meshing requirements for this case. Next, the numerical domain and mesh characteristics are described in more detail.

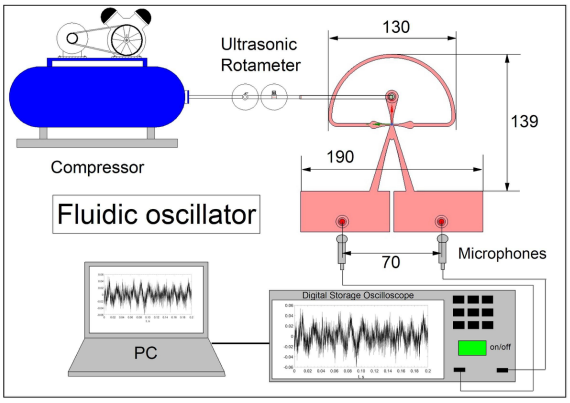

Figure 3. Experimental setup, scale in millimeters.

2.2 *Governing equations and numerical method*

Figure 2 shows the numerical domain (meshed using the software Gambit 3D®): the flow evolves on the same plane as the oscillator, with the exception of the inlet, which introduces the fluid perpendicular to the plane (from top to bottom, through the head). Note that the domain was extended beyond the ports (at the "man's feet") in order to avoid inconsistencies related to outlet boundary conditions. Moreover, this allowed for a more precise measurement of the outflow. The structured mesh elements are hexahedra, so orthogonality corrections are not needed in most of the domain. The near-wall regions are refined in order to resolve the boundary layer (y^+=5 for the nearest node to the wall), with a growth rate of b=1.1 starting at the fifth node from the wall (in general, it was observed that the boundary layer comprised at least five nodes). The total number of nodes in the numerical domain is 405,847. The boundary conditions are as follows: inlet condition at the "head", entering perpendicular to the "man's body". All surfaces inside the "little man" have a no-slip condition at the internal walls. The outlet (located far below the "feet" or ports) have a corresponding outlet condition of the constant pressure type. Note that the ports at both "feet" do not have any special boundary condition other than no-slip at the walls. These are measurement surfaces (far from the outlets) where the flow and velocity are recorded to a log file.

The inlet velocities are shown on Table 1, along with the respective Reynolds number, defined as:

$$Re = \frac{\rho U D}{\mu} \tag{3}$$

where D is the inlet diameter and U is the inlet velocity (referred to cross-sectional area of the circular inlet).

2.3 *Experimental setup*

Figure 3 shows the experimental device, which has the dimensions indicated in Figure 1.

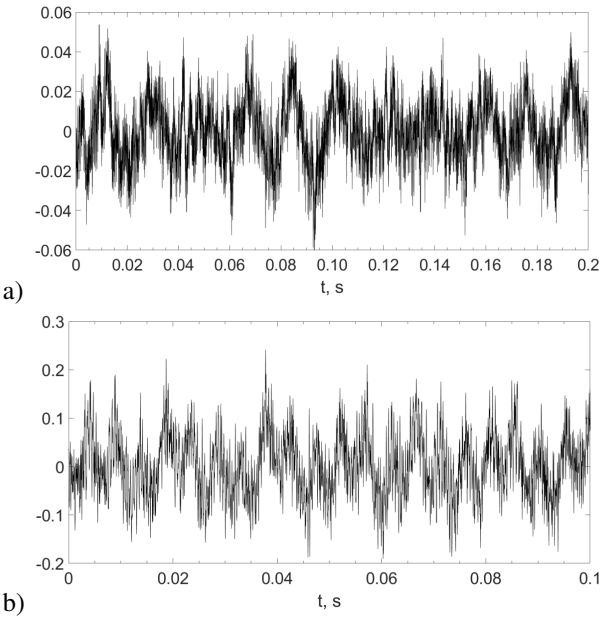

Figure 4. Sound signals obtained by the microphone for an air inlet velocity of a) 45 m/s for 0.2 s and b) 87 m/s for 0.1 seconds.

This device was made on a 3D printer (Ender-3 V2). The input of the oscillator is connected to a compressor air (4 hp power) with a capacity of 240 L, the air flow was monitored using an electronic flow control valve brand IFM model SD5500. The output signal was recorded with a high sensitivity microphone. A typical signal is shown in Figure 4 for an air inlet velocity of 45 m/s and 87 m/s.

3 Simulation results

Figure 5 shows the velocity field (arrows) superimposed to the pressure (colors) inside the fluidic oscillator. The inlet velocity here is 30 m/s, and the subfigures correspond to different times, at intervals of 0.025 seconds up to t=0.2 s. It is evident from the figures, that there is always a preferential flow through one of the outlets. Some of the consecutive images show the largest flow passing through the same outlet; this is because the oscillation frequency is larger than 0.025 s. The largest speeds are located at the entrance of the mixing region (upper body), in the vicinity of the control ports (arms). On t=0.025 s a low pressure region causes the formation of a recirculation zone on the outlet 1 (lower) channel, causing a hydrodynamic blockage and redirecting most of the flow through outlet 2 (upper). At a later time t=0.050 s, the low pressure (recirculation) has switched to the other side, sending most of the flow through outlet 1.

The switching is caused by the control ports (arms), which are connected, and the velocity (and pressure) difference between them is transmitted

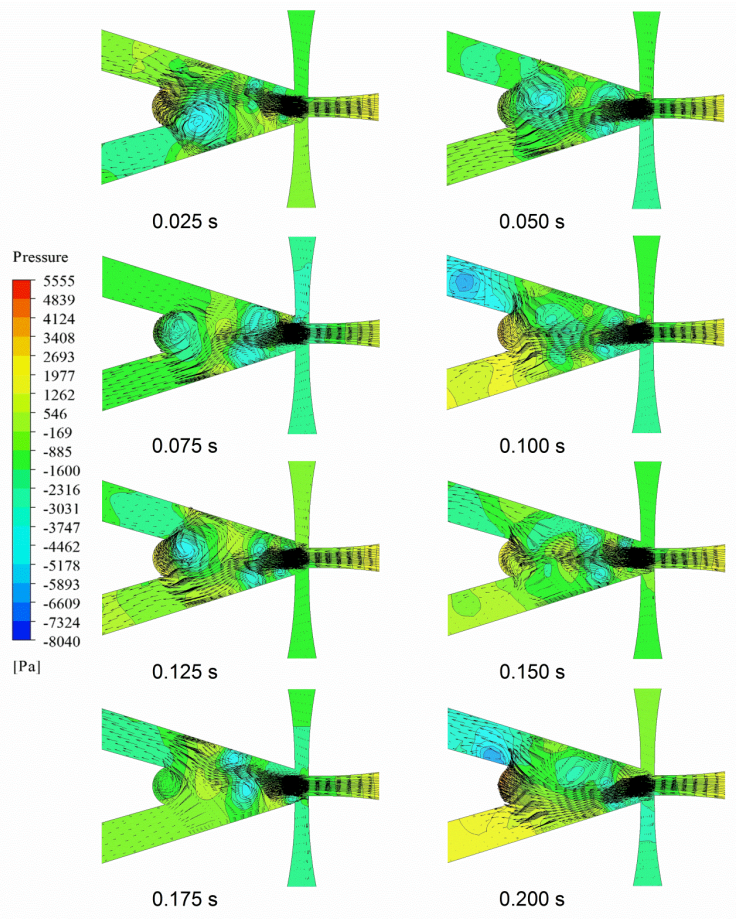

Figure 5. Velocity vector field at an air inlet velocity of 30 m/s for different times in seconds.

(feedback) causing the recirculation (and the fluid jet) to switch sides periodically. The large speed at the control ports (shoulders) makes them more sensitive to these perturbations, resulting in a self-sustained oscillation. The frequency depends mostly on the length or the channel (arms) that connects both control ports (hands), which in this case is constant (0.27 m). The inner workings of the oscillator are better appreciated when the streamlines are shown. Note that this is an unsteady problem, and the pathlines do not coincide with the streamlines, however they are an excellent visualization tool. Figure 6 shows the same time frames as in Figure 5, with the streamlines (the colors correspond to the local speed). It is clear from this representation how the flow travels preferentially through one output due to the recirculation at the "belly", and here it is clear how the flow passes through the control ports (arms). When this "control signal" reaches the other side (t=0.050 s), it causes the recirculation (and preferential jet) to switch sides. Note the presence of a smaller recirculation near the control port, always on the side of the preferential flow (Coanda effect). The pressure perturbation caused by this small vortex "pulls" the jet against the wall. If the inlet velocity is low, the perturbation at the entrance of the control port (vortex near the hand) will not be enough to cause the flow to switch sides.

Figure 7 shows, from top to bottom, the mass flow, pressure and mean velocity at the ports 1 (black) and 2 (blue). The columns correspond to: (a) inlet velocity of 5 m/s and (b) inlet velocity of 30 m/s. It is clear from the column (a) that the conditions near the control ports are not sufficient to cause the flow to switch. The 5 m/s does not create a perturbation strong enough to transmit the perturbation to the other control port (hand) and modify the flow symmetry. Although, Figure 7a shows no switching or oscillation (there is noise present, but no switching), the flow is not symmetric. Outlet 1 shows a mean mass flow of q_1=1.0E-04 kg/s and outlet q_2=-4.0E-04 kg/s (plotted negative, for visualization purposes). The velocity is significantly greater at port 2. Similar behavior was observed for the pressure and mean velocity.

Conversely, Figure 7b shows a case (mean inlet velocity of 30 m/s) where it is clear that the flow is switching between ports; the signal presents rapid oscillations of approximately constant period, close to T_c= 0.01 s, and a larger crossing period of about T_c= 0.035 s, where the blue and black signals cross the mean flow value of about q_c=0.0010 kg/s symmetrically; this is where the flow transitions to the other leg (outlet).

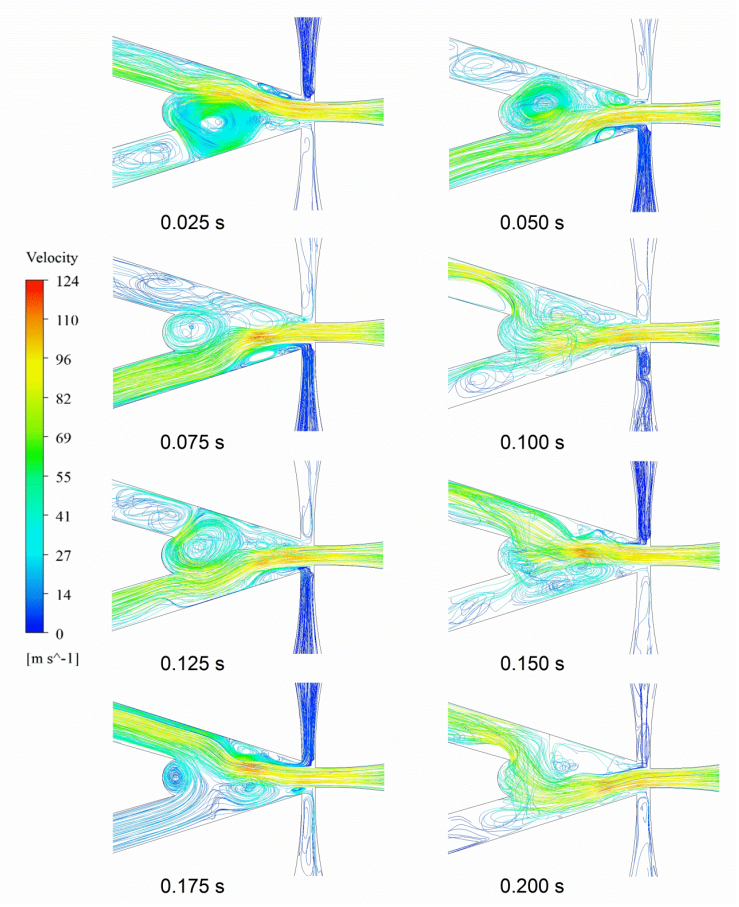

Figure 6. Velocity vector field at an air inlet velocity of 30 m/s for different times in seconds.

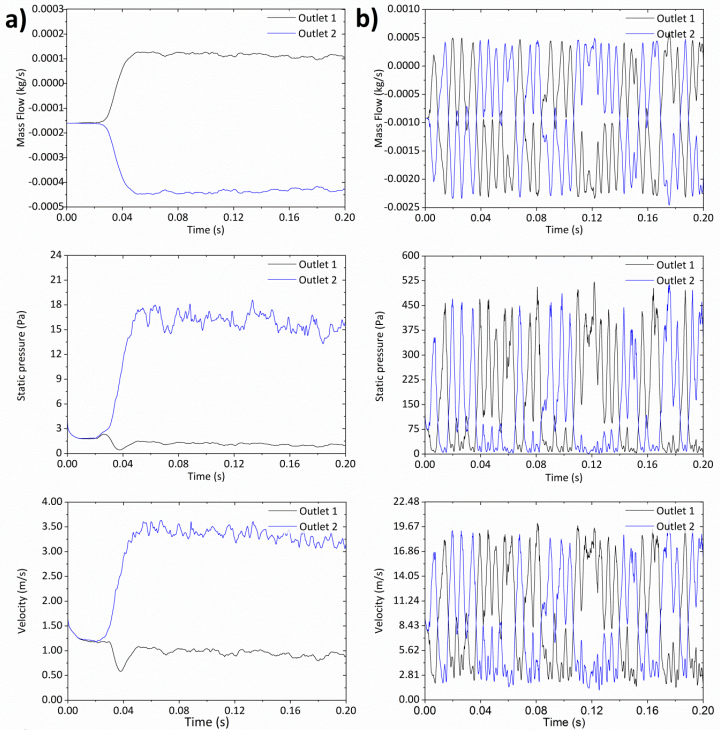

Figure 7. Fluctuations in mass flow, static pressure and velocity for air inlet at a) 5m/s and b) 30m/s.

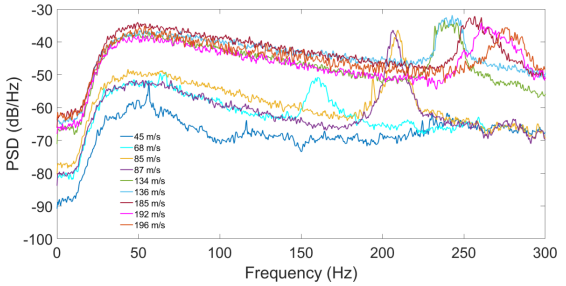

Figure 8. Frequencies present in the system at different air inlet velocities in a range of 45 m/s to 196 m/s.

Again, similar behavior was observed for the pressure (with a mean crossing value or about p_c=75 Pa) and velocity (mean crossing point around v_c=8.43 m/s). One can interpret these two periods of frequencies as corresponding to the large vortex at the mixing zone, and the larger period (switching) to the feedback from the arms, respectively, which can be observed as perturbations propagating through the arms as the flow switches side, in a video visualization of the case where U=30 m/s (provided with the supplementary materials, online version).

4 Experimental results

Concerning the experimental results, the output signals recorded with the microphone were transformed to the frequency domain using the Fast Fourier Transform (FFT), and analyzed using the Power Spectral Density (PSD) representation. The curves showed identifiable peaks that correspond to the switching frequency, which can be compared with the simulations. Frequency analysis allowed for the identification of the switching frequencies of the recorded signals from the experiments, which were very noisy.

Figure 8 shows the signals PSD obtained with the experimental prototype shown in Figure 3, for air inlet velocities in the range of 45 to 196 m/s. One can observe clearly identifiable peaks at approximately 160 Hz and 276 Hz, corresponding to U=68 m/s and U=87 m/s respectively. In Figure 9, the experimental frequency data obtained by a fast Fourier transform (FFT) and those obtained by simulation (signals of mass flow rate, pressure and velocity) are compared ca. It n be verified that as the Reynolds number increases, the oscillator frequency increases as well, which presents the frequency as a function of velocity, calculated with the switching period as previously explained. The solid circles correspond to the experiments, while the squares, diamonds and crosses correspond to frequencies obtained from the mass flow, static pressure and inlet velocity signals, respectively. The agreement is good, which can be interpreted as a correct detection of the crossing period

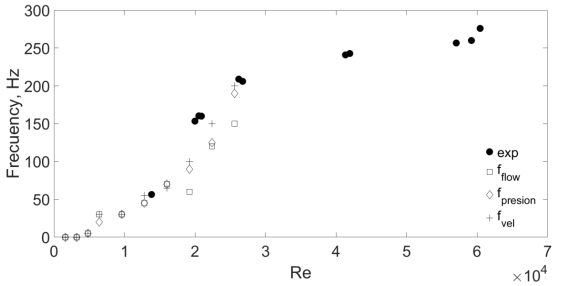

Figure 9. Comparison between the simulation and experimental frequencies with respect to the air inlet velocity. Filled circles - experimental data. Squares, diamonds and crosses - frequencies obtained from the mass flow, pressure and velocity signals respectively.

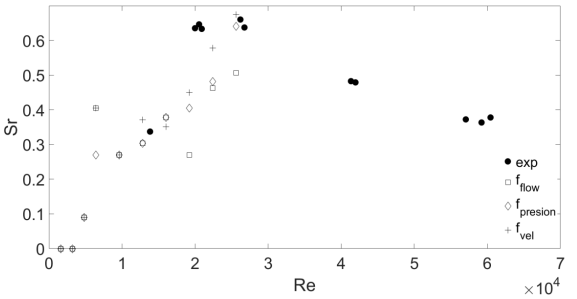

Figure 10. Strouhal number as a function of Reynolds number.

method, in agreement with the evidence obtained from the video (see supplementary materials online version).

This relationship can be cast in terms a dimensionless frequency or Strouhal number, defined as follows:

$$Sr = \frac{fL}{U} \tag{4}$$

where f corresponds to the oscillation frequency (obtained with the measured Tc), L is the distance between the control ports (hands) that defines the oscillation frequency (L=0.27 m). Figure 10 shows the Strouhal number Sr as a function of the Reynolds number Re, in the same format as Figure 9. Three oscillation regimes are observed.

Conclusion

This study investigated a 3D fluidic oscillator through Direct Numerical Simulation (DNS) and experimental prototyping. A particular design (man-shaped) that relies on a feedback loop (arms) causes a self-sustained switching between two outlets (the legs). It was observed the appearance of two important vortices that help redirect most of the flow through one of the outlets; a small vortex that "sticks" the jet of fluid to a wall redirecting most the flow through one outlet

(Coanda effect) and a large vortex in the "belly" that causes an hydrodynamic blockage on the other outlet.

Switching frequencies up to 276 Hz were determined across a Reynolds number range of 4800 to 60430. Below Reynolds number 4800, no fluctuations were observed in either the numerical or experimental signals. Within the range 4800 < *Re* < 25000, the Strouhal number exhibited a monotonically increasing relationship with the Reynolds number for the specific design under consideration. The governing variable influencing the output oscillation frequency in this design is the air inlet velocity, increasing up to a Reynolds number of 25000. Beyond this threshold, a transition regime was identified, after which the velocity's influence on frequency diminished. For *Re* > 25000, a decrement in the Strouhal number was observed, resulting in quasi-constant frequency values. This phenomenon is attributed to a resonance effect induced by feedback, as described by Tesar (2015), and further supported by McDonough et al. (2017) using liquids of varying viscosities.

Numerical simulation enabled the visualization of the Coanda effect (wall attachment of the oscillator's jet). Additionally, the formation and movement of low-pressure vortex structures, influenced by the feedback channel, were observed, leading to flow switching frequencies.

This mixed experimental and numerical study confirmed a functional oscillator design capable of producing frequencies up to 287 Hz. An essential consideration is determining the Reynolds number associated with the transition, where the marginal advantage of increasing frequency must be weighed against increased air consumption. This transitional zone is also linked to shear stresses in the feedback channel (Tesar, 2015).

Implementing numerical simulations of a fluidic oscillator to assess the frequency-to-mass-flow-rate curves serves as a preliminary step for a microbubble production scheme. Additionally, the generation of microbubbles through fluidic oscillators has been linked to enhanced interface area, which can influence heat and mass transfer processes in various applications (Tesař, 2021). Exploring various flow regimes is crucial from both scientific and engineering standpoints. The features of the oscillating outflow hinge on two key parameters, Reynolds number (Re) and Strouhal number (Sr). This study employs a blend of experimental and numerical methodologies to characterize these flow patterns and their associated regimes. Further investigation on the subject is recommended, with the perspective of more comprehensive Re number ranges and different geometries, as well as the connection with the resulting multiphase flows and fluidics.

Acknowledgements

The authors respectfully acknowledge SNI-CONACYT, CIC-UMSNH, UAdeC, as well as the UNAM-DGAPA-PAPIIT IN103321 Grant. This work would have not been possible without the technical support of Jesús Vargas Correa.

References

Bobusch, B. C., Woszidlo, R., Bergada, J. M., Nayeri, C. N., & Paschereit, C. O. (2013). Experimental study of the internal flow structures inside a fluidic oscillator. Experiments in fluids, 54, 1-12. doi: 10.1007/s00348-013-1559-6

Campagnuolo, C. J., & Lee, H. C. (1969). Review of some fluid oscillators (p. 0044). US Army Material Command, Harry Diamond Laboratories. https://apps.dtic.mil/sti/tr/pdf/AD0689445.pdf

Cerretelli, C., & Kirtley, K. (2009). Boundary layer separation control with fluidic oscillators. doi:10.1115/1.3066242

Devatine, A., & Mietton-Peuchot, M. (2009). A mathematical approach for oxygenation using micro bubbles: Application to the micro-oxygenation of wine. Chemical Engineering Science, 64(9), 1909-1917. doi:10.1016/j.ces.2009.01.012

Figueroa-Espinoza, B., & Legendre, D. (2010). Mass or heat transfer from spheroidal gas bubbles rising through a stationary liquid. Chemical Engineering Science, 65(23), 6296-6309. doi:10.1016/j.ces.2010.09.018

Ghanami, S., & Farhadi, M. (2019). Fluidic oscillators' applications, structures and mechanisms–a review. Challenges in Nano and Micro Scale Science and Technology, 7(1), 9-27. doi: 10.22111/TPNMS.2018.25051.1153

Gregory, J., & Tomac, M. N. (2013). A review of fluidic oscillator development and application for flow control. In 43rd AIAA fluid dynamics conference (p. 2474). doi: 10.2514/6.2013-2474

Gokoglu, S., Kuczmarski, M., Culley, D., & Raghu, S. (2010, June). Numerical studies of a supersonic fluidic diverter actuator for flow control. In 5th Flow control conference (p. 4415). doi: 10.2514/6.2010-4415

Gregory, J., & Tomac, M. N. (2013). A review of fluidic oscillator development and application

for flow control. In 43rd AIAA fluid dynamics conference (p. 2474). doi: 10.2514/6.2013-2474

Griffin, W. S. (1966). Design of a Fluid Jet Amplifier with Reduced Receiver: Interaction-region Coupling (Vol. 3651). National Aeronautics and Space Administration. https://ntrs.nasa.gov/api/citations/19660028389/downloads/19660028389.pdf

Jentzsch, M., Taubert, L., & Wygnanski, I. (2019). Using sweeping jets to trim and control a tailless aircraft model. AIAA Journal, 57(6), 2322-2334. doi: 10.2514/1.J056962

Jeong, H.-S., & Kim, K.-Y. (2017). Shape optimization of a feedback-channel fluidic oscillator. Engineering Applications of Computational Fluid Mechanics, 12(1), 169–181. doi: 10.1080/19942060.2017.1379441

Kim, G. H. (2011). A study of fluidic oscillators as an alternative pulsed vortex generating jet actuator for flow separation control (Doctoral dissertation, The University of Manchester (United Kingdom)). shorturl.at/dhlCM

Kim, S. H., Kim, H. D., & Kim, K. C. (2019). Measurement of two-dimensional heat transfer and flow characteristics of an impinging sweeping jet. International Journal of Heat and Mass Transfer, 136, 415-426. doi: 10.1016/j.ijheatmasstransfer.2019.03.021

Koklu, M. (2016). Effect of a Coanda extension on the performance of a sweeping-jet actuator. AIAA Journal, 54(3), 1131-1134. doi: 10.2514/1.J054448

Krüger, O., Bobusch, B. C., Woszidlo, R., & Paschereit, C. O. (2013). Numerical Modeling and Validation of the Flow in a Fluidic Oscillator. 21st AIAA Computational Fluid Dynamics Conference. doi: 10.2514/6.2013-3087

Lee S. Y., (1968) Fluid Control - Components and Systems, Technivision Services, Maidenhead, UK.

Löffler, S., Ebert, C., & Weiss, J. (2021). Fluidic-oscillator-based pulsed jet actuators for flow separation control. Fluids, 6(4), 166. doi: 10.3390/fluids6040166

López-Saucedo, F., Pecina-Treviño, E., la Garza-Rodríguez, D., Ramos-Méndez, K., Camacho-Ortegón, L., & Equihua-Guillén, F. (2016). Efecto de soluciones de KI, NaCl, MgCl2 y Na2SO4 en la distribución de tamaños de burbuja y surelación con la flotación de partículas de carbón y materia mineral. Revista Mexicana de Ingeniería Química, 15(1), 221-229. http://rmiq.org/iqfvp/Pdfs/Vol.%2015,%20No.%201/Mat2/Mat2.html

Lubert, C. (2011). On some recent applications of the coanda effect. International Journal of Acoustics and Vibration, 16(3), 144. doi: 10.20855/ijav.2011.16.3286

Menter, F.R.; Kuntz, M.; Langtry, R. (2003). Ten years of industrial experience with the SST turbulence model. Turbul. Heat Mass Transf., 4, 625–632. shorturl.at/oyF67

Mohammadshahi, Shabnam & Samsam-Khayani, Hadi & Nematollahi, Omid & Kim, Kyung. (2019). Flow Characteristics of a Wall-Attaching Oscillating Jet over Single-wall and Double-Wall Geometries. Experimental Thermal and Fluid Science. 112. 110009. doi: 10.1016/j.expthermflusci.2019.110009

Moukalled, F., Mangani, L., & Darwish, M. (2016). The finite volume method in computational fluid dynamics, Fluid Mechanics and its Applications. Cham: Springer, 113. doi: 10.1007/978-3-319-16874-6

Patankar S.V., Spalding D.B. (1972) A calculation procedure for heat, mass and momentum transfer in three-dimensional parabolic flows. Int J Heat Mass Transf 15(10):1787–1806.

Patankar, S. V. (1980). Numerical heat transfer and fluid flow, Hemisphere Publ. Corp., New York, 58, 288.

Quijano, G., Franco-Morgado, M., Córdova-Aguilar, M. S., Galindo, E., & Thalasso, F. (2020). Oxygen transfer in a three-phase bubble column using solid polymers as mass transfer vectors. Revista Mexicana de Ingeniería Química, 19(Sup. 1), 483-494. doi: 10.24275/rmiq/Proc1486

Rehman, F., Medley, G. J., Bandulasena, H., & Zimmerman, W. B. (2015). Fluidic oscillator-mediated microbubble generation to provide cost effective mass transfer and mixing efficiency to the wastewater treatment plants. Environmental research, 137, 32-39. doi: 10.1016/j.envres.2014.11.017

Schmidt, H. J., Woszidlo, R., Nayeri, C. N., & Paschereit, C. O. (2017). Separation control with fluidic oscillators in water. Experiments in Fluids, 58, 1-17. doi: 10.1007/s00348-017-2392-0

Tajik, A. R., Kara, K., & Parezanović, V. (2021). Sensitivity of a fluidic oscillator to modifications of feedback channel and mixing chamber geometry. Experiments in Fluids, 62, 1-19. doi: 10.1007/s00348-021-03342-0

Tomac, M. N., & Gregory, J. W. (2014). Internal jet interactions in a fluidic oscillator at low flow rate. Experiments in Fluids, 55, 1-14. doi: 10.1007/s00348-014-1730-8

Tomac, M. N. (2020). Novel impinging jets-based non-periodic sweeping jets. Journal of Visualization, 23, 369-372. doi: 10.1007/s12650-020-00633-2

Whalen, E. A., Shmilovich, A., Spoor, M., Tran, J., Vijgen, P., Lin, J. C., & Andino, M. (2018). Flight test of an active flow control enhanced vertical tail. AIAA Journal, 56(9), 3393-3398. doi: 10.2514/1.J056959

Wen, X., Li, Z., Zhou, L., Yu, C., Muhammad, Z., Liu, Y., ... & Liu, Y. (2020). Flow dynamics of a fluidic oscillator with internal geometry variations. Physics of Fluids, 32(7). doi: 10.1063/5.0012471

Woszidlo, R., Nawroth, H., Raghu, S., & Wygnanski, I. (2010, June). Parametric study of sweeping jet actuators for separation control. In 5th flow control conference (p. 4247). doi: 10.2514/6.2010-4247

Zimmerman, W.B, Tesar, V., Butler, S., & Bandulasena, H. (2008). Microbubble Generation. Recent Patents on Engineering, 2(1), 1–8. doi: 10.2174/187221208783478598

Zimmerman, W.B., Tesař, V., & Bandulasena, H. H. (2009). Efficiency of an aerator driven by fluidic oscillation. Part 1: Laboratory bench scale studies. Sheffield University. shorturl.at/lANR8